PHYSICAL REVIEW B **86**, 054103 (2012)

Simulation of alloy thermodynamics: From an atomic to a mesoscale Hamiltonian

T. Garnier,[1] A. Finel,[2] Y. Le Bouar,[2] and M. Nastar[1]
[1]*CEA, DEN, Service de Recherches en Metallurgie Physique, F-91191 Gif-sur-Yvette, France*
[2]*LEM, CNRS-ONERA, BP72 - 29 Avenue de la Division Leclerc, F-92322 Châtillon, France*
(Received 11 April 2012; published 2 August 2012)

Starting from an atomic interaction model of an alloy with a clustering tendency, a mesoscopic thermodynamic simulation method is developed. The alloy is represented by a mesoscopic rigid lattice of cells characterized by the number of solute atoms they contain and a discrete cellular Monte Carlo (CMC) algorithm is designed to perform simulations at this scale. The central quantity is a mesoscopic free energy, whose components (local free energy and stiffness parameter) are extracted from the equilibrium properties of single-cell and two-cell systems. Particular attention has been paid to properly incorporate, at mesoscale, the correlations between neighboring cells with identical concentrations. Finally, the ability of the CMC method to compute thermodynamic properties such as phase diagrams, interface profiles, and equilibrium fluctuation spectra is illustrated on a model alloy as well as on an Ising model with interactions up to the second-nearest neighbors, previously developed for body-centered-cubic Fe-Cu alloys. The very good agreement between the CMC calculation results for different cell sizes and direct computations at the atomic scale indicate that the proposed scale change is thermodynamically consistent.

DOI: 10.1103/PhysRevB.86.054103 PACS number(s): 05.10.Ln, 81.30.−t, 64.60.Q−, 64.70.kd

I. INTRODUCTION

Microstructures of alloys determine to a large extent their physical and mechanical properties. A quantitative description of their evolution can now be achieved using atomic kinetic Monte Carlo simulations based on a vacancy diffusion mechanism.[1–3] While they provide impressive results on the early stages of a two-phase separation and ordering kinetics, they are rapidly limited by the cost of CPU time and fail to predict late-stage kinetics. The study of the alloy behavior at later time and larger scale is, however, essential to get a better understanding of microstructures.

In dilute systems, a multiscale approach coupling density functional theory calculations, atomic kinetic Monte Carlo models, and mesoscale methods such as cluster dynamics[4] and event-based Monte Carlo[5] makes the link between diffusion mechanisms and long-term microstructure evolutions. However, a similar approach remains to be done for concentrated alloys. An efficient way to predict microstructural evolutions at large scale is provided by coarse-grained methods such as the phase field one.[6–9] The main advantage of these approaches is that they are free from any restriction on the spatiotemporal correlations in microstructure evolutions which, for concentrated alloys, play a major role. The precise aim of this paper is to propose and validate a coarse-graining procedure that, first, derives an effective cellular Hamiltonian from the atomic scale, and, second, uses this Hamiltonian in a mesoscopic Monte Carlo algorithm.

In general, coarse-grained methods consist of dividing a solid into mesoscopic cells and writing kinetic equations for the evolution of the cell concentrations, assuming that a local equilibrium is established in every cell at the characteristic time scale of the microstructure evolution. This procedure leads to a mesoscopic master equation where the driving force is derived from a coarse-grained free-energy functional of the Ginzburg-Landau type.[10,11]

Recently, following this route, a complete derivation of phase field equations from the atomic scale has been proposed for phase-separating systems with a kinetics based on first-nearest-neighbor direct exchanges.[12] The obtained mesoscopic kinetic model was able to quantitatively describe a precipitation kinetics involving a nucleation and growth mechanism. In this approach, all of the ingredients (chemical potentials, mobilities, stiffness coefficient, and noise terms) are derived from a numerical coarse-graining procedure and therefore depend on the coarse-graining size. In addition, this derivation has made clear that the stiffness coefficient significantly depends on the local concentration, whereas this concentration dependence is usually neglected in the classical phenomenological approach. This stiffness coefficient is extracted from the concentration fluctuation spectrum of a macroscopic system at equilibrium. However, this approach is only valid for homogeneous states and cannot therefore be used inside the miscibility gap. In that region, the value of the stiffness coefficient is extrapolated using a low-order polynomial. The accuracy of this procedure decreases at low temperature when solubility limits are small because the concentration range in which the thermodynamic states are homogeneous is very limited.

An important point of the present paper is to propose and validate an alternative procedure to compute the stiffness coefficient down to low temperature. Another aspect of the present work is to use a coarse-grained free energy into a discrete Monte Carlo approach, i.e., the cellular Monte Carlo (CMC) method, which operates directly at the scale of the mesoscopic cells. In other words, the mesoscopic kinetics equations retain the nonlinear relation between the temporal derivatives of the evolving cell concentrations and the thermodynamic driving forces. Therefore, this approach may still be valid when the chosen cell size is not large enough to justify the Fokker-Planck approximation of the mesoscopic master equation needed to derive a stochastic phase field model.[12]

In the present work, this discrete and stochastic mesoscopic method is validated not only on thermodynamic properties

©2012 American Physical Society

such as the phase diagram, equilibrium interface profiles, and equilibrium fluctuation spectra, but also on the finite-size calculation of the free energy, including inside the miscibility gap. The first system studied is a binary model alloy with a body-centered-cubic (bcc) structure, first-nearest-neighbor interactions, and a clustering tendency. A second application is the Fe-Cu alloy for which the atomic interaction model extends to second-nearest-neighbor interactions. Its main characteristic from a theoretical point of view is its simplicity: it is a typical unmixing system, with a large and almost symmetrical miscibility gap where size effects due to the atomic radius differences are negligible. As a consequence, it has been frequently studied as a benchmark case to test the validity of models of phase-transformation kinetics: nucleation and growth theory,[13] cluster dynamics (see Ref. 4, and references therein), and Monte Carlo simulations.[14–16]

Section II is dedicated to the presentation of the CMC method. In Sec. III, we introduce a local parametrization method based on a Widom procedure[17,18] to calculate cell free energies using both an atomic Monte Carlo (AMC) method and an analytical approach for the stiffness evaluation. In Sec. IV, the resulting thermodynamic properties of the model alloy predicted by the CMC method are compared to direct AMC simulations. In Sec. V, the efficiency of the parametrization procedure combined with the CMC algorithm is illustrated on the Fe-Cu system.

II. MONTE CARLO ALGORITHM: FROM THE ATOMIC TO THE MESOSCOPIC SCALE

A. AMC simulations

In the present framework, the thermodynamic description is restricted to atomic-scale configurations on a rigid lattice where each node is occupied by an atom. The atomic interactions may be associated to each local cluster: pairs, tetrahedra, etc. They are usually parameterized on *ab initio* calculations (e.g., Ref. 2). We consider an alloy of atoms A and Boccupying N sites of a bcc lattice and restrain ourselves to pair interactions, leading to a simple Ising Hamiltonian:

$$\mathbb{H} = \frac{1}{2} \sum_{\{\alpha,\beta)\in(A,B\}} \sum_{l} \sum_{(i,j)\in[\![1,N]\!]^2} \gamma_{ij}^{l} V_l^{\alpha\beta} n_i^{\alpha}\left(1-n_j^{\beta}\right), \qquad (1)$$

where γ_{ij}^{l}, the adjacency matrix, is equal to 1 if sites i and j are the lth nearest-neighbor (NN) sites. $n_i = 1$ if site i is occupied by a B atom, and 0 otherwise. $V_l^{\alpha\beta}$ is the pair interaction between atoms α and β located on the lth NN sites. As we considered pair interactions only, the properties of the system are invariant by the transformation $c \rightarrow 1-c$, where c is the total concentration in solute atoms B.

Starting from an initial configuration, other configurations in the phase space are explored using a Monte Carlo algorithm,[19] i.e., the Metropolis algorithm[20] in the present case. Next, the Hamiltonian is truncated to first-NN interactions, with only repulsive heterointeractions $V_1^{AB} > 0$. Such a system displays a complete miscibility at high temperature. At a temperature $T = T_c$, a second-order phase transition occurs, and at lower temperature, a miscibility gap related to a first-order phase transitions appears. As a consequence, at low temperature, phase interfaces are sharp, while they broaden close to T_c.

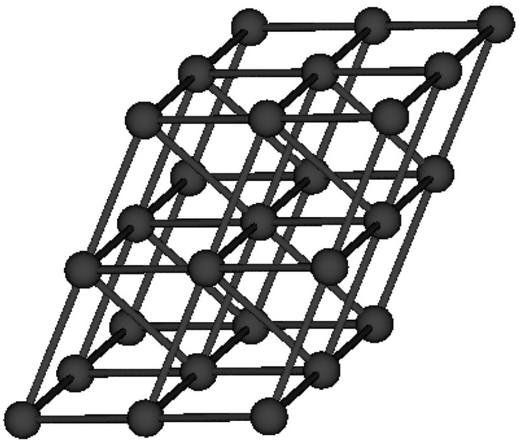

FIG. 1. Representation of an assembly of 27 atoms linked by first-NN bounds, forming a $d = 3$ rhombohedric cell.

B. Principles of CMC simulations

In cellular Monte Carlo (CMC) simulations, a bcc crystal is divided into cells of linear dimension d in units of first-NN distance. We choose to divide the bcc solid into rhombohedral cells with faces parallel to the $(110)_{BCC}$, as they are the planes of lowest surface energy in the case of a first-NN interaction model. As a consequence, the cellular lattice is not homothetic to the atomic one. The cellular lattice is a rhombohedral lattice, and a representation of the rhombohedral cell can be found in Fig. 1. To any atomic-scale configuration $\{n_i\}$, we can associate a mesoscopic configuration $\{N_n\}$, where $N_n = \sum_{i\in n} n_i$ is the total population of solute atoms B in the cell n, which can take d^3+1 different discrete values. The canonical partition function Z can be written as

$$Z = \sum_{\{N_n\}} \sum_{\{n_i\}/\{N_n\}} e^{-\beta\mathbb{H}(\{n_i\})} = \sum_{\{N_n\}} e^{-\beta\Gamma^d(\{N_n\})}, \qquad (2)$$

where $\beta = (kT)^{-1}$ is the inverse temperature. The sum over $\{n_i\}$ at a given $\{N_n\}$ corresponds to an integration of the short-range modes of wavelength $\ell < d$. The functional $\Gamma^d_{(\{N_n\})}$ is a free energy that reduces to the original Hamiltonian if $d = 1$, and is equal to the total free energy if d is the size of the system. Concerning microscopic properties, it is a free energy of the short modes that have already been integrated out. Concerning macroscopic properties, it can be formally considered as an effective Hamiltonian for the long-range modes that have not been integrated out yet. An objective of this work is to propose a controlled procedure to evaluate this mesoscopic Hamiltonian Γ^d.

Γ^d is a function of the whole set $\{N_n\}$. As the atomic system displays short-range interactions only, it makes sense to consider a cluster expansion of this function restricted to first-NN cell interactions:

$$\Gamma^d(\{N_n\}) \approx \sum_{n} E^d(N_n) + \sum_{n,m} \gamma_{n,m} \Lambda^d_{N_n,N_m}, \qquad (3)$$

where $E^d(N_n)$ is the local free energy of a cell n of population N_n, and $\Lambda^d_{N_n,N_m}$ is the interaction energy between first-NN cells n and m. $E^d(N_n)$ is such that $\Gamma^d(\{N_n\}) = E^d(N_1)$ for a system made of a single cell with periodic boundary conditions (PBC). For a given cell size, the accuracy of the expansion in Eq. (3) is expected to decrease when the correlation length ξ increases, with the latter corresponding to the characteristic length at which site occupancies affect each others. When ξ is smaller than the cell size, the site correlations are almost all included in the local free energy $E^d(N_n)$ and the cell interaction energy terms $\Lambda^d_{N_n,N_m}$. In the opposite case, for example close to the critical temperature where the correlation length diverges, it should be less justified to consider first-NN cell interaction energies only.

As in AMC, a Monte Carlo approach can be used to explore the energy landscape associated with the cellular Hamiltonian. In the present case, the metropolis algorithm is used. Moreover, only discrete conservative exchanges between cells $(N_n,N_m) \rightarrow (N_n+1,N_m-1)$ are considered. The corresponding CMC algorithm consists of the following steps:

(1) randomly drawing a couple of cells (n,m),

(2) computing the energy difference, $\Delta\Gamma = \Gamma^d(N_n+1,N_m-1) - \Gamma^d(N_n,N_m)$,

(3) drawing a random number $R \in [0,1]$,

(4) if $R < (e^{-\beta\Delta\Gamma})$, then accept the exchange.

The formal continuity between the CMC and AMC simulations is obvious: an AMC simulation is a CMC simulation with only one site per cell. Taking into account the discrete nature of exchanges allows one to study contiguity problems such as percolation phenomena within a vacancy mediated kinetics, as it allows discontinuities of the concentration field. Additionally, the master equation is not approximated by a Fokker-Planck equation, allowing for a more accurate description of the fluctuations.[21]

III. PARAMETERIZATION METHOD

In this section, we present the procedure to calculate the energy parameters of the cellular Hamiltonian. A Widom integration method is employed to calculate the cell local free energies, and exact free-energy calculations are performed to estimate the cell interactions.

A. Local free energy of a single cell

The Widom integration scheme is a computational tool employed to calculate chemical potentials.[17,18,22] Originally written in the lattice gas formalism, it can as well be applied on rigid lattice models of alloys. The canonical partition function of an alloy with N solute atoms is written as a function of the energy of a system with $(N-1)$ solute atoms, obtaining this way the alloy chemical potential (see Appendix A). The Widom scheme combined with AMC simulations is applied to a small simulation box identical to a single cell with PBC. An integration of the resulting chemical potential leads to the free energy F_N of a cell of population N. As defined in Sec. II, the latter corresponds to the cell local free energy $E^d(N) = F_N$. This method is very efficient, especially when cells are small: the number of concentrations to explore scales as d^3.

The precision on the local free energy is estimated by calculating the relative difference between two independent computations of the alloy chemical potential using Eqs. (A5) and (A7) presented in Appendix A. In order to get a relative error below 10^{-3}, the number of Monte Carlo steps (MCS, number of exchange attempts per site) to reach and explore equilibrium and the number of energies to be measured has to be specified. At temperatures not too close to the critical temperature ($|T-T_c|/T_c > 0.1$), 10 000 MCS to reach equilibrium and around 50 000 energy calculations per site with one MCS between each calculation allows one to reach a relative error of 10^{-3}.

B. Interaction energy term

Concentration gradient terms between two cells are linked to the interaction energy terms [see Eq. (3)]. It is a tremendous work to compute all of the interaction energies, as their number evolves as d^6. For two given cells with populations N and M, we therefore consider the Taylor expansion of the interaction energy at the average population between the cells with respect to the concentration difference:

$$\Lambda^d_{N,M} \approx \Lambda^d_{\frac{N+M}{2},\frac{N+M}{2}} + \frac{1}{2}\lambda^d_{\frac{N+M}{2}}\frac{(N-M)^2}{d^6} + \cdots . \tag{4}$$

The zeroth-order term is a homogeneous term which depends on the average concentration. It is related to the boundary condition applied during the calculation of the local free energy. The first-order term disappears for obvious symmetry reasons: the energy cannot depend on the orientation of the lattice.

In the present work, we choose not to focus on the case of a second-order transition where the correlation length is large. Our purpose is to find a convenient way to parametrize the cellular interactions when correlations are small enough. In this limiting case, the Taylor expansion may be limited to the second-order term. In the continuous limit of Eq. (4), the interaction term would be approximated by $\Lambda^d_{N_n,N_m} = \lambda|\nabla N|^2$, and the CMC effective Hamiltonian would tend toward the Cahn-Hilliard free-energy functional[23] widely used in phase field methods.

The stiffness coefficient λ^d_N is, of course, size dependent. This size dependency can be analyzed through the normalized stiffness coefficient κ defined as follows:

$$\kappa^d_N = \lambda^d_N * \frac{6}{Z_{\text{cell}}}, \tag{5}$$

where Z_{cell} is the total number of first-NN bonds going out of the cell. While in a simple cubic atomic lattice, the number of bounds between two cells is d^2, in the case of a bcc lattice, it slightly differs at small d. There is a total of $Z_{\text{cell}} = 12d^2 - 6d + 2$ bounds going out of the cell: two bounds per atom on each face, plus a correction as the atoms on the six broad angle edges have three bounds going out while belonging to two faces, and a corner correction for the two atoms belonging to three such edges. As we consider first-NN cellular interactions only, the effective number of bounds between two cells is the total number of atomic bounds going out of the cell divided by the number of faces, i.e., six in the present case.

1. Correction of the periodic boundary conditions

The local free-energy term, noted E_N^d in Eq. (3), is computed by considering a single cell with PBC. Therefore, it does not incorporate all of the fluctuations that exist between two neighboring cells constrained to have the same concentration but not the same atomic configurations. The free-energy contribution associated with these additional fluctuations corresponds in Eq. (4) to the zeroth-order term $\Lambda_{N,N}^d$, hereafter referred to as *periodic boundary correction term.*

In order to compute this quantity, a coupled Widom integration scheme is designed on a two-cell system: an atomic system with PBC is divided into two closed subsystems of the size of a cell. Atoms are not allowed to cross the interface but they interact through it. The homogeneous interaction term is extracted from the Widom integration of such a coupled system with the same concentration on both sides. The Widom integration is performed simultaneously on both subsystems (the calculation is detailed in Appendix B). Due to the PBC, the two subsystems interact through two interfaces of $2d^2$ bounds each. The energy correction per bound of the interface is then $\frac{\Delta E}{4d^2}$, where ΔE is the difference between the energy computed on the coupled system and twice the one derived from the single-cell Widom integration scheme. The boundary correction term is then $\Lambda_{N,N}^d = \frac{Z_{\text{cell}}}{6}\frac{\Delta E}{4d^2}$.

2. Stiffness parameter

A method has been proposed to compute the stiffness coefficient λ_N^d. It is based on a fitting procedure of the coarse-grained AMC fluctuation spectra.[12] According to this procedure, an atomic configuration obtained by an AMC simulation is divided into cells. Average concentrations of cells are calculated and the fluctuation spectrum of the cell concentration field $S_d(\mathbf{k})$ is measured:

$$[\beta S_d(\mathbf{k})]^{-1} = \frac{1}{\langle L^3 |\tilde{c}_d(\mathbf{k})|^2\rangle}, \tag{6}$$

where $\tilde{c}_d(\mathbf{k})$ is the discrete Fourier transform of the local cell concentration field, L is the linear size of the simulation box, and $\mathbf{k} = \frac{2\pi}{L}(n,m,p)$ with $(n,m,p) \in [\![0,\frac{L}{d}-1]\!]^3$ is a vector in the reciprocal cell lattice. This quantity is then averaged over many configurations. In the hypothesis of small Gaussian fluctuations, the stiffness λ_N^d characterizing the cell interactions is obtained from the slope of the inverse fluctuation spectrum when plotted as a function of $|\mathbf{k}|^2$ by a fit in the linear regime (small $|\mathbf{k}|^2$). Typically, 10^5 MCS are performed to equilibrate the system. They are followed by 8×10^5 spectrum measurements with one MCS between each. This yields an average spectrum from which the stiffness λ_N^d is extracted. The resulting normalized stiffness parameter κ_N^d is deduced from it according to Eq. (5). An example of the calculation at $T = 1.5T_c$ is shown in Fig. 2. $d\kappa_N^d$ is found to increase linearly with d for cell sizes up to $d = 5$. Therefore, this result indicates that away from the critical temperature, the main size effect is the geometrical factor introduced in Eq. (5) down to the smallest sizes we investigated here.

In the miscibility gap, the equilibrium state is a system decomposed in two phases of concentrations equal to the solubility limits. Concentrations of the cells used to calculate the fluctuation spectrum fluctuate around the solubility limits as well. Nonetheless, the applicability of the method described above, which is valid only for homogeneous equilibrium states, is limited. We propose here an alternative method based on the exact free-energy calculation of dilute finite-size systems, which avoids these drawbacks. Again we consider a two-cell system with PBC. The free energy of the system is denoted $F_{N,M}^d$, where N and M correspond to the solute number of the cells, while F_N^d is the free energy of a single cell with PBC. We deduce from both free energies the coupling free energy, $Fc_{N,M}^d = F_{N,M}^d - F_N^d - F_M^d$. This system is similar to two interacting first-NN cells, but due to the PBC they interact through two interfaces of $2d^2$ bounds each. Taking into account the fact that κ_N^d is almost independent of d, we can then write

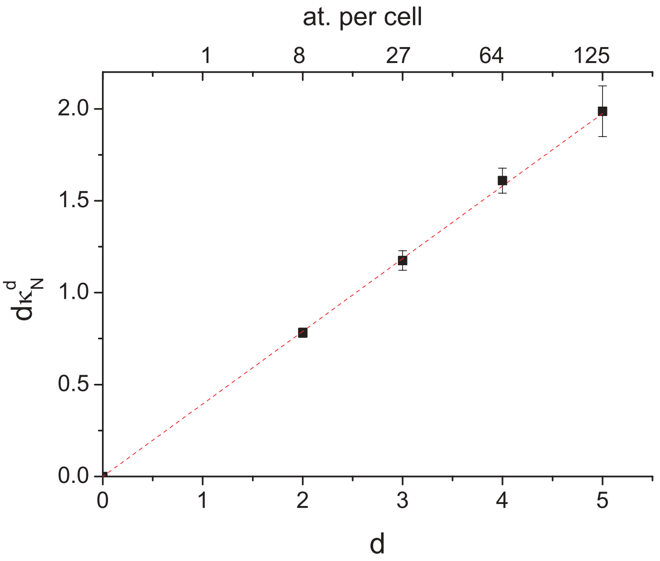

FIG. 2. (Color online) Cellular stiffness extracted from fits of the AMC fluctuation spectra at $T = 1.5T_c$, $c = 0.2$ and different cell sizes d. Squares are the stiffness parameters extracted from AMC values, while the dashed line corresponds to a linear fit.

$$Fc_{N,M}^d - Fc_{\frac{N+M}{2},\frac{N+M}{2}}^d = \frac{2}{2d^2}\kappa_{\frac{N+M}{2}}\frac{(N-M)^2}{d^6}. \tag{7}$$

Using the definition of the coupling energy, we obtain

$$\frac{1}{d^8}\kappa_{\frac{N+M}{2}}(N-M)^2 = F_{N,M}^d - F_N^d - F_M^d - \left(F_{\frac{N+M}{2},\frac{N+M}{2}}^d - 2F_{\frac{N+M}{2}}^d\right). \tag{8}$$

In the dilute case, where $N = 2$ and $M = 0$, we finally get

$$\frac{4}{d^8}\kappa_1 = F_{2,0}^d - F_2^d - F_0^d - \left(F_{1,1}^d - 2F_1^d\right). \tag{9}$$

Details of the calculation are explained in Appendix C. One can force the cells to have a concentration in the miscibility gap. However, the approach is limited by the complexity of the calculation when the number of solute atoms included in the two-cell system increases. Despite this limitation, a large range of concentration can be explored, overcoming the limitation by the use of the fact that κ_N^d is almost d

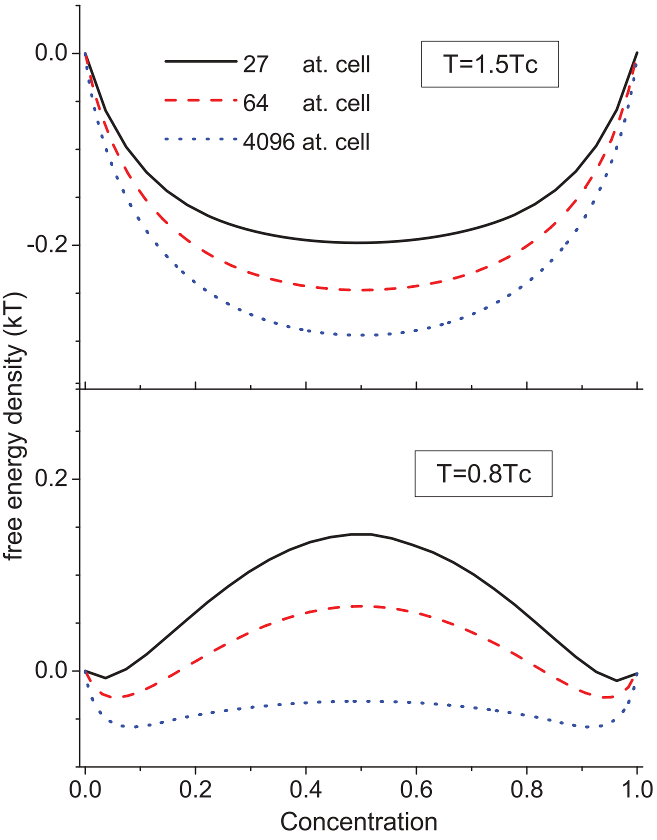

FIG. 3. (Color online) Reduced free energy per atom calculated by means of the Widom scheme applied on a first-NN atomic interaction model for various cell sizes, at $T = 1.5T_c$ (top) and $T = 0.8T_c$ (bottom).

independent. By varying the cell size, concentrations up to $c = 0.125$ can be reached. These results can then be interpolated using a polynomial fit to obtain the stiffness at any concentration.

C. Numerical results

Figure 3 shows the local free-energy density computed with the Widom scheme for different cell sizes. The local free-energy density is definitely size dependent, as it was observed in earlier works.[22,24] We also note a continuous concentration dependency of the local free energy for all sizes investigated here. In all cases, the free energy is decreasing with the cell size. This last result could be expected considering the free energy from a variational point of view: the equilibrium state of a system is the one that minimizes its free energy with respect to the configuration probability density, i.e., the fluctuation probability. When the system size increases, the fluctuation range increases and therefore the free energy can be further minimized.

The analytical method to calculate the stiffness parameters in the limiting case of dilute systems provides one with a few discrete values at concentrations up to $c = 0.125$. To get the values over the entire concentration range, an interpolation between the known values is needed. The symmetry property of the stiffness implies the use of an even function. As the calculated stiffness parameters present a non-negligible concentration dependency, at least a second-order polynomial is required to fit them. However, as no exact calculation is available in the concentrated region, the use of a polynomial with an order larger than four induces spurious oscillations in the concentrated region. Therefore, we use the highest polynomial fit with a monotonous derivative: a fourth-order polynomial fit (cf. Fig. 4).

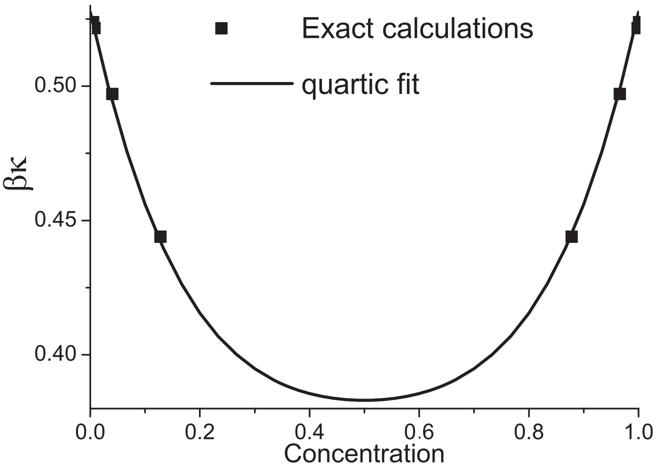

FIG. 4. Reduced mean interaction per bound of a first-NN atomic interaction model at $T = 1.5T_c$. The squares are the exact calculation and the solid line is the polynomial extrapolation.

IV. MACROSCOPIC PROPERTIES

The parametrization procedure of the cellular Hamiltonian is validated by comparing several macroscopic properties computed by CMC simulations with the reference ones obtained by AMC simulations. For this purpose, a benchmark system is considered, where atoms sit on a bcc lattice and interact through first-nearest-neighbor interactions. Three thermodynamic properties are explored: the fluctuation spectrum, the phase diagram, and the interface profile. In addition to these properties, the free energy of finite-size systems is investigated to test the cellular Hamiltonian at intermediate concentrations in the miscibility gap.

A. Phase diagram

To estimate the solubility limits of the phase diagram, equilibrium two-phase systems are simulated in the canonical ensemble. When the simulation box is large enough, concentrations at the end of the equilibrium profile correspond to the solubility limits. The simulations are performed in a $2 * 64^3$ cell box. As observed in Fig. 5, where phase diagrams for two different cell sizes are presented, the CMC results are in very good agreement with the reference AMC phase diagram. While the mean-field approximation gives good results at low concentrations only ($c < 0.01$), the CMC phase diagram sticks to the AMC one at all temperatures. A more quantitative comparison is presented in Fig. 6, where the relative difference between solubility limits obtained by CMC simulation or mean field and the reference AMC simulation result is shown. Near T_c, the quality of the CMC results slightly decreases.

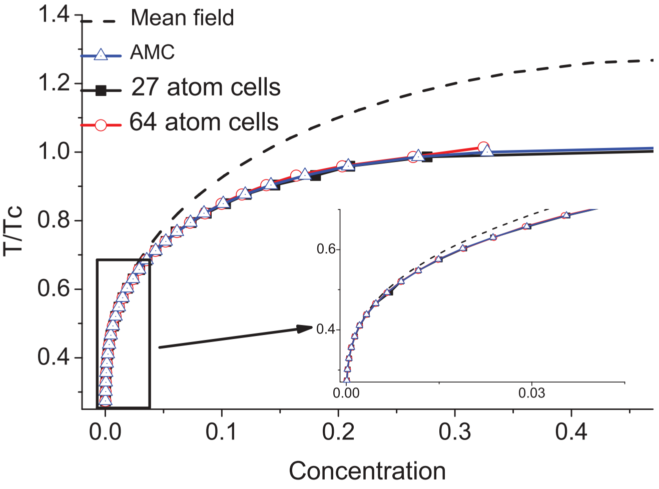

FIG. 5. (Color online) Phase diagram of a first-NN interaction model obtained by AMC and CMC simulations. The small window is a zoom of the phase diagram at low temperature. The dashed line is the mean-field approximation. T_c is the critical temperature of the AMC system.

However, the agreement with the AMC solubility remains good: while the mean-field approximation predicts a critical temperature with a relative error of about 20%, the relative error of the CMC method on T_c does not exceed 3%. Thus, the approximation made in Eq. (3) appears to be relevant for our current problem. Finally, the importance of the correction to the boundary condition discussed in Sec. III B1 is shown in Fig. 7 by displaying the relative difference between solubility limits obtained by CMC simulations with and without this correction and the reference AMC simulation result. The relative error on the solubility limit in CMC simulations is reduced by one order of magnitude by considering the boundary correction.

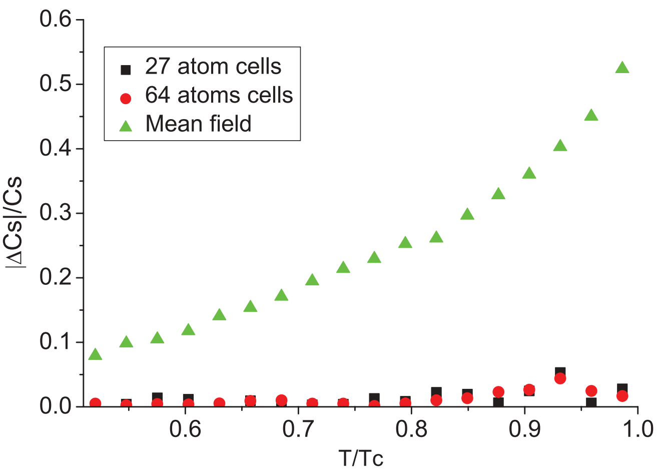

FIG. 6. (Color online) Effect of the cell size on the relative differences between the solubility limit obtained by CMC calculations with 27 atom cells (black) and 64 atom cells (dark gray) or by a mean-field approximation (light gray) and the AMC one. T_c is the critical temperature of the AMC system.

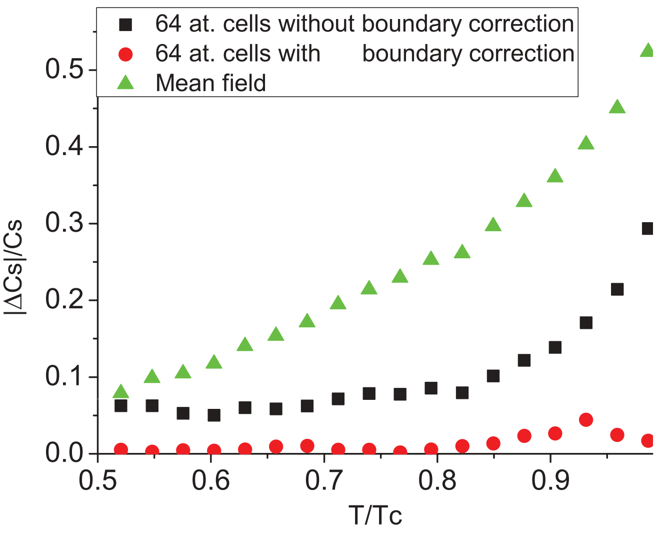

FIG. 7. (Color online) Effect of the boundary correction on the relative differences between the solubility limit obtained by CMC calculations with 64 atom cells, including the boundary correction (dark gray), without the boundary corrections (black), or by the mean-field approximation (light gray) and the AMC one.

B. Fluctuation spectrum

The fluctuation spectrum $S_d(\mathbf{k})$ can be measured on AMC simulations according to the procedure detailed in Sec. III B2 as well as on CMC simulations. The comparison between the two is an important test of the CMC parametrization since it shows both short-range and long-range fluctuation features. As shown in Figs. 8 and 9, the comparison is performed by measuring the relative difference between CMC and AMC fluctuation spectra. A systematic study is performed at various concentrations and for temperatures in the range $T \in [0.6T_c, 2T_c]$. It shows that a good agreement over the whole spectrum is achieved in all circumstances, with a maximum discrepancy below 10% and which increases near

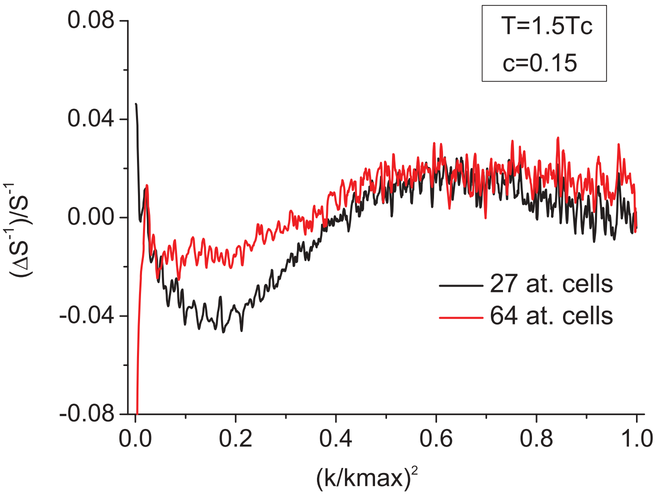

FIG. 8. (Color online) Relative difference between AMC and CMC fluctuation spectra with respect to the AMC spectrum at a concentration $C = 0.15$ and a temperature $T = 1.5T_c$ with cells of 27 atoms (black) and 64 atoms (red). $k_0^2 = 3(\frac{2\pi}{d})^2$.

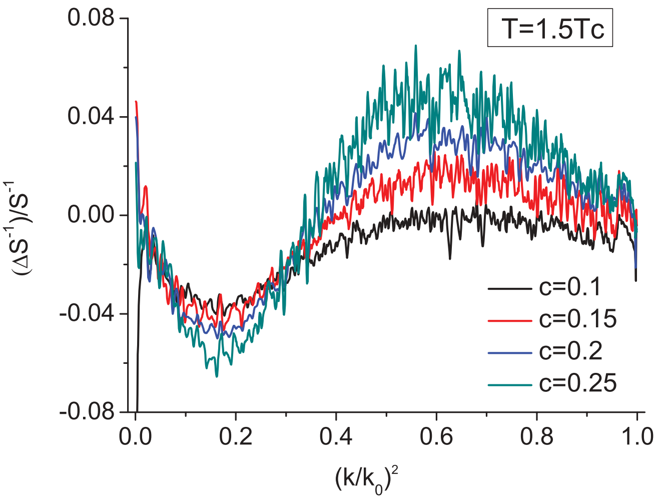

FIG. 9. (Color online) Relative difference between AMC and CMC fluctuation spectra with respect to the AMC spectrum at various concentrations and a temperature $T = 1.5T_c$ with cells of 64 atoms. $k_0^2 = 3(\frac{2\pi}{d})^2$.

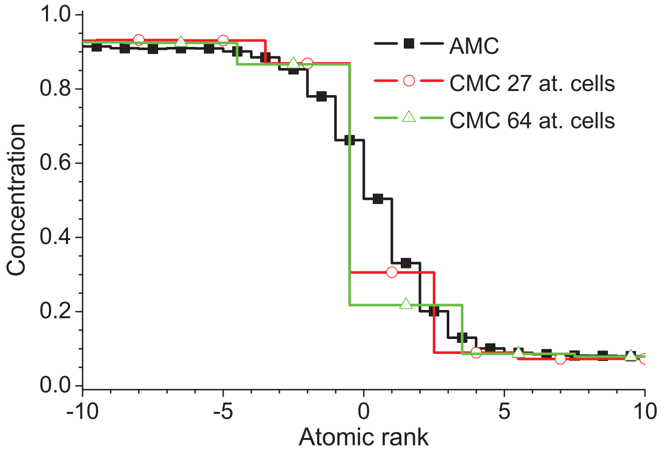

FIG. 10. (Color online) Interface profiles calculated by the AMC and CMC method for various cell sizes at $T = 0.8T_c$ on a $2 \times (64)^3$ site system. The average concentration in a $(110)_{BCC}$ plane is given as a function of the atomic rank.

the solubility limit. The lone points at very low k come from the poor statistics in this area.

It is not possible to measure fluctuations of a homogeneous system at intermediate concentrations in the miscibility gap, since a phase separation would occur. As a consequence, the parametrization in this area cannot be validated by this test.

C. Interface profile

The simulation of an interface profile using a CMC method allows checking the cellular Hamiltonian on a large range of concentration: from the solubility limits to the unstable region. An equilibrium two-phase system is simulated using an AMC simulation in the canonical ensemble with a box of 2×64^3 atoms, using two pure phase separated by a $(110)_{BCC}$ plane as the initial condition. The resulting interface profile is obtained by averaging the concentration in each $(110)_{BCC}$ plane after equilibration and comparing to the corresponding CMC one. It is well known that a two-dimensional interface in a three-dimensional system may display a roughening transition at a temperature T_R: for $T < T_R$, the interface is thin and pinned on the lattice, whereas for $T > T_R$, it is rough, wanders across the lattice, and its width increases with its longitudinal size. Concerning the present analysis, the coarse-grained simulations should produce the complete thermodynamic behavior of the interface, whether roughening fluctuations are present or not.[25] As can be observed in Fig. 10 and in Table I, the interfaces of a few atomic ranks are correctly described at the cellular scale. More specifically, with a coarse-graining size close to half the interface width (cells of 64 atoms), the accuracy of the interface width is better than 10%.

TABLE I. Parameters of the interface profile at $T = 0.8T_c$ for various cell sizes. The interface profile is fitted with the function $c(x) = 0.5 + (c_s - 0.5)\tanh(\frac{x}{2B})$.

d^3	c_s	±	B	±
1	0.08	0.01	1.19	0.02
27	0.07	0.01	1.05	0.05
64	0.08	0.01	1.09	0.06

D. CMC free energy of a finite-size system

The alloy chemical potential of a CMC system can be integrated to obtain the total free energy of the CMC system, as was done for an AMC system in Sec. III A. By this method, the free energy can be computed at any concentration, including inside the miscibility gap, and allows one to check the accuracy of the method in this area, which was out of range for the fluctuation measurement (cf. Sec. IV B). For this purpose, the Widom integration scheme has been adapted to the CMC algorithm (cf. Appendix A).

In Fig. 11, the free energy of a single cell of 4096 atoms computed with the Widom scheme at the atomic scale is

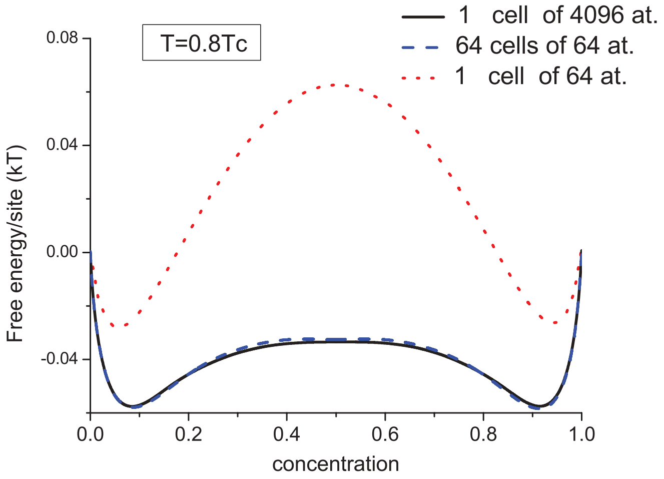

FIG. 11. (Color online) Free energy per site obtained by a Widom integration scheme of a single AMC box of 64 atoms (red dotted line), a single AMC box of 4096 atoms (black solid line), and a large CMC system of 64 cells of 64 atoms (blue dashed line), at temperature equal to $T = 0.8T_c$.

compared to the one computed with the Widom scheme applied to CMC simulations with 64 cells of 64 atoms. It shows that the total free energy is well reproduced by the CMC method, even in the concentration region of the miscibility gap. An additional curve corresponding to the free energy of a single cell of 64 atoms is plotted to emphasize again the dependency of the local free energy with the cell size (see also Fig. 3). The relative error between the AMC simulation and the equivalent CMC simulation with the same number of atomic sites is below 3%. To exemplify the reliability of CMC simulations with respect to AMC simulations in the miscibility gap, we discuss a specific point inside the miscibility gap and choose the spinodal limit for that purpose. The spinodal limit corresponds to the concentration value at which a change of sign of the first derivative of the free energy with respect to concentration occurs. The spinodal limit is thus a function of the size of the whole system. Thermodynamic consistency implies that AMC and CMC simulations should provide the same value of the spinodal limit if they are performed on a system with the same number of atomic sites. Performing simulations on a 4096 site box, the finite difference provides us with the first derivative of the chemical potential and thus the spinodal limit. A relative difference between CMC and AMC spinodal limit of around 5% was observed.

The stiffness parameter κ_N is crucial as it triggers phase transitions and controls microstructures of out-of-equilibrium systems. Therefore, in order to estimate the required accuracy for its calculation, the sensitivity of the free energy to errors on the measurement of the stiffness is investigated. Figure 12 shows that the free energy is sensitive to the stiffness parameter. While the effect of an increase of 20% of κ_N is hardly noticeable on the minimum of the free energy, its impact is important in the miscibility gap. Figure 12 shows that at $c = 0.5$, the disagreement with AMC simulation on the free energy is increased by a factor of two for an increase of κ_N by 20%. However, this disagreement remains limited compared to the depth of the well. On the other hand, we remind one that κ_N was extrapolated using a polynomial approximation (see Sec. III B2). The uncertainty of κ_N due to this polynomial approximation can be estimated to roughly 10%. Thus, taking into account the previous discussion, we can expect this error to be of little consequence on macroscopic properties.

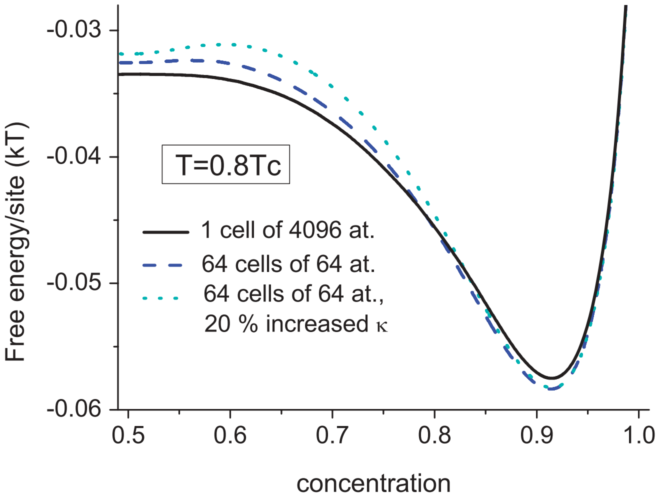

FIG. 12. (Color online) Free energy per site obtained by a Widom integration scheme of a single AMC box of 4096 atoms (black solid line), a CMC system of 64 cells of 64 atoms (blue dashed line), and the same with a stiffness κ increased by 20% (light-blue dotted line), at temperature equal to $T = 0.8T_c$.

V. APPLICATION TO FE-CU

Extensive *ab initio* calculations have already been performed on the Fe-Cu system,[2] which allowed one to build a set of first-NN and second-NN pair interactions. The corresponding AMC simulations were observed to be in good agreement with experimental thermodynamic and kinetic data. We consider here the same atomic interactions and again use them to validate the parametrization procedure and the CMC algorithm. Above $T \approx 1100\,\mathrm{K}$, the Fe-Cu alloy displays an allomorphic transformation from a body-centered-cubic to a face-centered-cubic structure. Since the rigid lattice does not allow allomorphic transformations, such a phase transition is completely ignored by the present AMC and thus CMC simulations.

A. The cellular Fe-Cu Hamiltonian

If the atomic Hamiltonian had been restricted to first-NN interactions, then the previous results could have been immediately employed by rescaling the temperature. The present study allows one to check if the parametrization procedure and the CMC algorithm still hold in a system including longer-range interactions.

We again use the coarse-graining procedure presented above. The mesoscopic cell interactions are limited to first-NN cells only. The cell local free energies and boundary correction terms are computed using, respectively, the Widom scheme and the coupled Widom scheme according to the parametrization procedure described in Sec. III. All quantities are used as input parameters of the CMC code without additional treatment. For various cell sizes, the interaction stiffness is derived from the analytical free-energy calculation of dilute two-cell systems. The resulting values are interpolated and extrapolated to higher concentrations using a parabolic fit.

B. The thermodynamic Fe-Cu properties

The phase diagram of the Fe-Cu system has been computed using both CMC and AMC simulations. As shown in Fig. 13, the overall agreement is very good. While the phase diagram of a mean-field model is correct only at low temperature, the phase diagram obtained with the CMC method is still good at high temperatures. However, the agreement obtained with the smallest cell of 27 atoms is not as satisfying as the one obtained in the situation described in Sec. IV, where the atomic Hamiltonian was limited to first-NN interactions (see Fig. 5). This loss of accuracy can be explained considering the size of the atomic interaction range. Indeed, the correlation length at the atomic scale increases with the range of the atomic interactions. Consequently, the precision of the coarse-graining procedure used here, in which the effective cell interactions are limited to first NN, will decrease for a given cell size when the atomic interaction range increases. Therefore, we can see in Fig. 13 that as soon as the cell has a

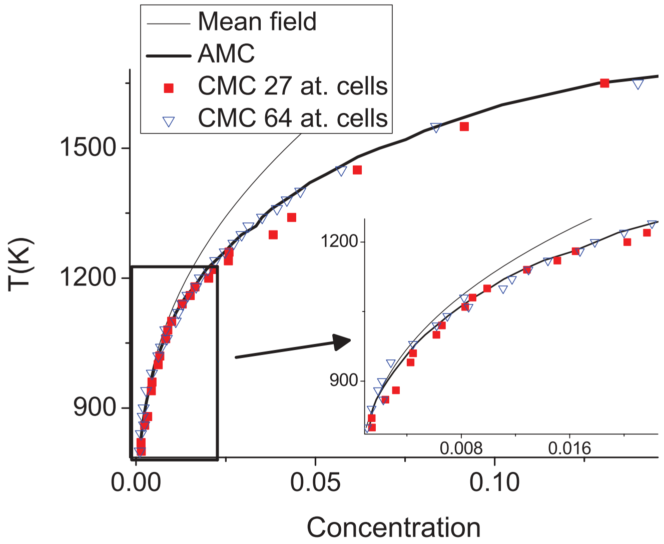

FIG. 13. (Color online) Phase diagram of the Fe-Cu system in the Fe-rich region obtained through AMC and CMC simulations. The small window shows a zoom of the dilute region. The thin line is the mean-field approximation, the broad one is the AMC result, and the symbols are the CMC results.

size of 64 atoms, the phase diagram is in much better agreement with the reference AMC one. This illustrates the fact that away from T_c, i.e., when the correlation length is finite, it is always possible to select a minimum cell size for which the coarse-grained procedure with effective interactions limited to first NN will reproduce accurately the overall thermodynamic behavior.

The fluctuation spectra of the Fe-Cu system are obtained using the same procedure as in Sec. III. Once again, as can be observed in Fig. 14 at $T = 1700$ K, a good overall agreement is obtained.

The study of the interface profile is consistent with the fluctuation spectra. As can be seen in Fig. 15, the interface profile at $T = 1550$ K is qualitatively correct. The measurement of the profile width by adjusting the classical function $c(x) = 0.5 + (c_s - 0.5)\tanh(\frac{x}{2B})$ on the profile shows that a semiquantitative agreement is obtained between CMC results for 27 and 64 atom cells and AMC results (see Table II).

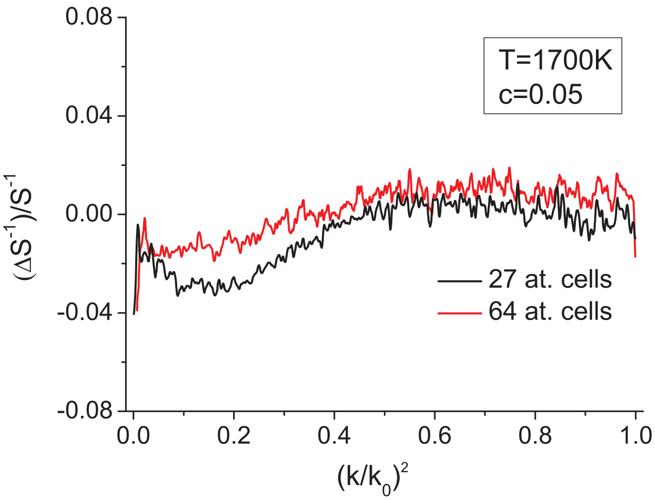

FIG. 14. (Color online) Relative difference between AMC and CMC fluctuation spectra with respect to the AMC spectrum at a concentration $c = 0.05$ and a temperature $T = 1700$ K with cells of 27 atoms (black) and 64 atoms (red). $k_0^2 = 3(\frac{2\pi}{d})^2$.

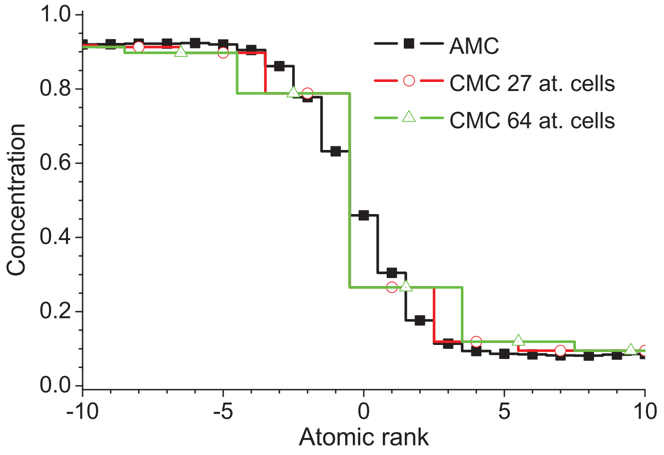

FIG. 15. (Color online) Equilibrium interface profile of the Fe-Cu system obtained with AMC simulation and CMC simulations at various cell sizes and at $T = 1550$ K.

Finally, we confirm that these results were obtained using the systematic parametrization procedure proposed in Sec. III A, without any free parameter. They show the reliability of our coarse-graining approach.

VI. CONCLUSION

To make a link between atomic and macroscopic simulations, a mesoscopic method based on a coarse-graining procedure that keeps the discrete aspect of atoms is presented: the cellular Monte Carlo algorithm. The parametrization procedure relies on an atomic lattice model of alloys. A cellular Hamiltonian is obtained using an AMC algorithm combined with a Widom integration scheme to get local free-energy terms associated with a single cell and direct free-energy calculations of a two-cell system for the stiffness parameter between cells. It is shown that this procedure allows for the determination of this mesoscopic stiffness parameter down to low temperature. This cellular Hamiltonian is directly incorporated into the CMC algorithm. This procedure keeps the nonlinear link between the temporal derivatives of the concentration field and the thermodynamic driving force. The overall procedure leads to quantitative simulations of the thermodynamic properties, such as the phase diagram, equilibrium fluctuations, or interface profiles. Also, the good

TABLE II. Parameters of the interface profile of the Fe-Cu system at 1550 K at various cell sizes. The interface profile is fitted with the function $c(x) = 0.5 + (c_s - 0.5)\tanh(\frac{x}{2B})$.

d^3	c_s	±	B	±
1	0.08	0.01	1.11	0.05
27	0.09	0.01	1.0	0.1
64	0.09	0.01	1.3	0.1

agreement between the AMC and CMC predictions of the free energies of finite-size systems provides a full validation of the parametrization method at cell concentrations not only in the stable region but also in the miscibility gap. It is emphasized that the CMC ingredients (cell free energy, periodic boundary correction term, and mesoscopic stiffness coefficient λ_N^d) are highly cell-size dependent.

As in phase field approaches, the CMC method tackles the simulation of concentrated as well as dilute alloys, whereas some other mesoscopic approaches of the thermodynamics of inhomogeneous systems are usually limited to a more restrained concentration range. Close to T_c, a better understanding of the variation of the cellular interaction energy with the concentration difference between cells and the cell size would be useful to improve the parametrization procedure. The application to the Fe-Cu alloy containing first-NN, but also second-NN, atomic interactions extends the validation of the method to longer-range interaction models. It can be extended easily to larger cluster interactions. Moreover, the coarse-graining procedure used to define the cellular Hamiltonian is not limited to rigid lattices. Continuous degrees of freedom, such as displacements around an average lattice, can be easily integrated within the Widom scheme. This would lead to a coarse-grained cellular Hamiltonian that embeds the free-energy contributions of atomic displacements. Also, if atomic size mismatch leads to a change of lattice parameter, then the long-range elastic interactions induced by coherency could be incorporated using the usual continuous elasticity theory, provided that the cells are large enough.

As an AMC algorithm corresponds to a CMC algorithm in the particular case of cells containing a single atom, an adaptive Monte Carlo algorithm would be easy to implement. The outcome will be the same cellular Hamiltonian, complemented by associated coarse-grained mobilities defined at the scale of the cells. The authors of Ref. 12 presented a procedure to derive coarse-grained mobilities from an atomic model of the direct exchange diffusion mechanism. This approach has to be generalized to describe realistic diffusion mechanisms such as the vacancy mediated mechanism.

ACKNOWLEDGMENTS

Part of this work has been funded by the European FP7 Perform project and the European fusion materials modeling program (EFDA). The authors want to thank Vasily Bulatov for the fruitful discussions they had at the very beginning of the project and Frédéric Soisson for his assistance with the AMC code and the modeling of Fe-Cu alloys.

APPENDIX A: WIDOM INTEGRATION SCHEME FOR AMC AND CMC SYSTEMS

The Widom integration scheme is presented here in the formalism of a binary alloy on a rigid lattice. We consider a lattice made of N_{tot} sites, either occupied by atoms of type A or B, with the latter being called the solute. Each configuration of the N solute atom system can be seen as a configuration of the $(N-1)$ solute atom system in which an A atom is changed into a B atom. Following this idea, we write the canonical partition function with N solute atoms as a function of the energy of a system of $(N-1)$ solute atoms plus the energy required to change an A into a B. Let Z_N be the canonical partition function of a N solute atom system, Ω_N its phase space, $\mathbb{H}_{\mathbf{n}}$ the value of its Hamiltonian in the configuration $\mathbf{n}$, and $\tau_{\mathbf{n}}$ the set of the positions where an A is available:

$$Z_N = \sum_{\mathbf{n}\in\Omega_N} e^{-\beta\mathbb{H}_{\mathbf{n}}}, \tag{A1}$$

$$Z_N = \sum_{\mathbf{n}\in\Omega_{N-1}} e^{-\beta\mathbb{H}_{\mathbf{n}}}\left(\sum_{j\in\tau_{\mathbf{n}}} e^{-\beta\Delta Ej^+} g^+\right), \tag{A2}$$

where ΔEj^+ is the energy required to change an A into a B on site j, and $(g^+)^{-1}$ is the number of times a given configuration is built this way. As a consequence, in general g^+ is a configuration-dependent quantity: $g^+ = g^+_{\mathbf{n},j}$. We can write that

$$\frac{Z_N}{Z_{N-1}} = \frac{\sum_{\mathbf{n}\in\Omega_{N-1}} e^{-\beta\mathbb{H}_{\mathbf{n}}}\left(\sum_{j\in\tau_{\mathbf{n}}} g^+_{\mathbf{n},j} e^{-\beta\Delta Ej^+}\right)}{\sum_{\mathbf{n}\in\Omega_{N-1}} e^{-\beta\mathbb{H}_{\mathbf{n}}}}. \tag{A3}$$

This is a thermodynamic average deduced from a $(N-1)$ solute atom system:

$$\frac{Z_N}{Z_{N-1}} = \left\langle \sum_{j\in\tau_{\mathbf{n}}} g^+_{\mathbf{n},j} e^{-\beta\Delta Ej^+} \right\rangle_{N-1}. \tag{A4}$$

As a result, we obtain the exchange chemical potential

$$\begin{aligned}\mu^{A\to B}_{(N-1)} &= F_N - F_{N-1}\\ &= -\beta^{-1}\ln\left\langle \sum_{j\in\tau_{\mathbf{n}}} g^+_{\mathbf{n},j} e^{-\beta\Delta Ej^+} \right\rangle_{N-1}.\end{aligned} \tag{A5}$$

In a similar way, we can build the $(N-1)$ solute atom partition function as a function of the N solute atom partition function and deduce from it the chemical potential

$$Z_{N-1} = \sum_{\mathbf{n}\in\Omega_N} e^{-\beta\mathbb{H}_{\mathbf{n}}}\left(\sum_{i\in\alpha_{\mathbf{n}}} e^{-\beta\Delta Ei^-} g^-_{\mathbf{n},i}\right), \tag{A6}$$

where $\alpha_{\mathbf{n}}$ is the set of sites occupied by a B atom in configuration $\mathbf{n}$, ΔEi^- is the energy required to turn a B into an A on site i, and $1/g^-_{\mathbf{n},i}$ is the number of times a given configuration is built this way. Using the same procedure as above, we then obtain

$$\begin{aligned}\mu^{B\to A}_{(N)} &= F_{N-1} - F_N\\ &= -\beta^{-1}\ln\left\langle \sum_{i\in\alpha_{\mathbf{n}}} g^-_{\mathbf{n},i} e^{-\beta\Delta Ei^-} \right\rangle_{N}.\end{aligned} \tag{A7}$$

In principle, if the thermodynamic averages are computed exactly, we have $\mu^{B\to A}_{(N)} = -\mu^{A\to B}_{(N-1)}$. However, due to the finite length of the Markov chain, a discrepancy may appear between the estimations of these two quantities.

For an AMC system, $g^+_{\mathbf{n},j}$ and $g^-_{\mathbf{n},i}$ are independent of the configuration:

$$g^-_{\mathbf{n},j} = \frac{1}{N_{\text{tot}} - (N-1)}, \quad g^+_{\mathbf{n},j} = \frac{1}{N}. \tag{A8}$$

In a CMC system, this is not the case: atoms of a given cell are undifferentiated and then the number of ways a cell may increase by one its number of solute atoms reduces to one. Similarly, while the set $\tau_{\mathbf{n}}$ is the set of positions of the A atoms in AMC, in CMC it is the set of the nonfull cells. Therefore, the g^+ term of Eq. (A5) becomes the inverse of the number of cells which have B atoms after the virtual addition of a solute atom B:

$$g_{\mathbf{n}}^{+} = \frac{1}{N_{\text{cell}} - N_{\text{empty}(\mathbf{n},j)}}, \tag{A9}$$

where N_{cell} is the total number of cells and $N_{\text{empty}(\mathbf{n},j)}$ is the number of empty cells in B after the virtual addition in the configuration ($\mathbf{n}$). We note that in the case of a single site cell, the AMC expression of g^+ is retrieved. Moreover, as in general in a CMC system $g_{\mathbf{n},j}^{+}$ is configuration dependent, it has to be computed for the various cell configurations which are explored during the thermodynamic averaging process.

APPENDIX B: WIDOM INTEGRATION OF TWO INTERACTING SYSTEMS

We consider a system made of two coupled subsystems. No particle exchange is allowed between them, but there are some chemical interactions between atoms of different subsystems, with every subsystem being identical to a single cell. Let $Z_{N,N}$ be the partition function of a coupled system of two N solute atom cells, $\Omega_N \otimes \Omega_N$ be its phase space, and $\mathbb{H}_{\mathbf{n}}$ be its Hamiltonian in the configuration $\mathbf{n}$. We then have the relationship

$$Z_{N,N} = \sum_{\mathbf{n}\in\Omega_N} \sum_{\mathbf{m}\in\Omega_N} e^{-\beta \mathbb{H}_{\mathbf{n},\mathbf{m}}}. \tag{B1}$$

Similarly as done previously, we can write the canonical partition function of the coupled system with $(N+1, N+1)$ solute atoms as a function of the Hamiltonian of a system of (N,N) particles. First we use the previous approach on one of the subsystems:

$$Z_{N+1,N+1} = \sum_{\mathbf{n}\in\Omega_N} \left[\sum_{\mathbf{m}\in\Omega_{N+1}} e^{-\beta \mathbb{H}_{\mathbf{n},\mathbf{m}}} \left(\sum_{k\in\tau_{\mathbf{n}}} e^{-\beta \Delta E k^{+}} g_{\mathbf{n},k}^{+} \right) \right]. \tag{B2}$$

Here, for example in an AMC system, $g_{\mathbf{n}}^{+} = \frac{1}{N+1}$. Then we apply the same approach on the second subsystem:

$$Z_{N+1,N+1} = \sum_{\mathbf{m}\in\Omega_N} \sum_{\mathbf{n}\in\Omega_N} e^{-\beta \mathbb{H}_{\mathbf{n},\mathbf{m}}} \times \left[\sum_{k\in\tau_{\mathbf{n}}} \sum_{l\in\tau_{\mathbf{m}}} (e^{-\beta\Delta E k^{+}} g_{\mathbf{n},k}^{+})(e^{-\beta\Delta E l^{+}} g_{\mathbf{m},l}^{+}) \right]. \tag{B3}$$

The resulting partition function ratio is then written as

$$\frac{Z_{N+1,N+1}}{Z_{N,N}} = \left\langle \sum_{k\in\tau_{\mathbf{n}}} \sum_{l\in\tau_{\mathbf{m}}} (e^{-\beta\Delta E k^{+}} g_{\mathbf{n},k}^{+})(e^{-\beta\Delta E l^{+}} g_{\mathbf{m},l}^{+}) \right\rangle_{N,N}. \tag{B4}$$

We deduce the free-energy difference:

$$\beta(F_{N+1,N+1} - F_{N,N}) = -\ln \left[\left\langle \sum_{l\in\tau_{\mathbf{n}}} \sum_{k\in\tau_{\mathbf{n}}} (e^{-\beta\Delta E k^{+}} g_{\mathbf{n},k}^{+})(e^{-\beta\Delta E l^{+}} g_{\mathbf{m},l}^{+}) \right\rangle_{N,N} \right]. \tag{B5}$$

By carrying out this calculation at every cell concentration, one gets the homogeneous interaction term.

APPENDIX C: EXACT CALCULATION IN THE DILUTE LIMIT OF THE FREE ENERGY

In the dilute limit, exact cellular free energies can be easily calculated. The interaction stiffness can be computed from the values of F_1, F_0, $F_{1,1}$, and $F_{2,0}$. Let Z_1 (Z_2) be the number of neighbors in the first (second) shell. Considering that in a cell of size d, there are d^3 sites and, as a consequence, $\frac{d^3(d^3-1)}{2}$ ways to put a pair of solute atoms into it, we define Y_1 (Y_2) as the number of configurations among them, where the two atoms are first (second) NN. Similarly, in a two-cell system with PBC, there are $\frac{d^3(d^3-1)}{2}$ configurations with two, and only two, solute atoms in the same cell. We define in such a case W_1 (W_2) the number of configurations among them where the two atoms are first (second) NN. Finally, in a two-cell system with PBC, there are d^6 configurations with a single solute atom in each cell, and we define X_1 (X_2) as the number of configurations among them where the two atoms are first (second) NN. Using the definition of the free energy as the logarithm of the partition function, we obtain

$$\begin{aligned} F_{2,0} = -\beta^{-1} \ln \Bigg\{ & \left[\frac{d^3(d^3-1)}{2} - W_1 - W_2 \right] e^{-\beta V_1^{AB}(2Z_1)} \\ & \times e^{-\beta V_2^{AB}(2Z_2)} + W_1 e^{-\beta V_1^{AB}[2(Z_1-1)]} e^{-\beta V_2^{AB}[2(Z_2)]} e^{-\beta V_1^{BB}} \\ & \times e^{-\beta V_1^{AA}} + W_2 e^{-\beta V_1^{AB}(2Z_1)} e^{-\beta V_2^{AB}[2(Z_2-1)]} e^{-\beta V_2^{BB}} \\ & \times e^{-\beta V_2^{AA}} \Bigg\} - \beta^{-1} \ln \big[e^{-\beta V_1^{AA}(2Z_1/2d^3-2Z_1)} \\ & \times e^{-\beta V_2^{AA}(2Z_2/2d^3-2Z_2)} \big], \end{aligned} \tag{C1}$$

$$\begin{aligned} F_{1,1} = -\beta^{-1} \ln \big[& (d^6 - X_1 - X_2) e^{-\beta V_1^{AB} 2Z_1} e^{-\beta V_2^{AB} 2Z_2} \\ & + X_1 e^{-\beta V_1^{AB} 2(Z_1-1)} e^{-\beta V_2^{AB} 2(Z_2)} e^{-\beta V_1^{BB}} e^{-\beta V_1^{AA}} \\ & + X_2 e^{-\beta V_1^{AB} 2(Z_1)} e^{-\beta V_2^{AB} 2(Z_2-1)} e^{-\beta V_2^{BB}} e^{-\beta V_2^{AA}} \big] \\ & - \beta^{-1} \ln \big[e^{-\beta V_1^{AA}(2Z_1/2d^3-2Z_1)} e^{-\beta V_2^{AA}(2Z_2/2d^3-2Z_2)} \big], \end{aligned} \tag{C2}$$

$$\begin{aligned} F_2 = -\beta^{-1} \ln \Bigg\{ & \left[\frac{d^3(d^3-1)}{2} - Y_1 - Y_2 \right] e^{-\beta V_1^{AB} 2Z_1} e^{-\beta V_2^{AB} 2Z_2} \\ & + Y_1 e^{-\beta V_1^{AB} 2(Z_1-1)} e^{-\beta V_2^{AB} 2(Z_2)} e^{-\beta V_1^{BB}} e^{-\beta V_1^{AA}} \\ & + Y_2 e^{-\beta V_1^{AB} 2(Z_1)} e^{-\beta V_2^{AB} 2(Z_2-1)} e^{-\beta V_2^{BB}} e^{-\beta V_2^{AA}} \Bigg\} \\ & - \beta^{-1} \ln \big[e^{-\beta V_1^{AA}(Z_1/2d^3-2Z_1)} e^{-\beta V_2^{AA}(Z_2/2d^3-2Z_2)} \big], \end{aligned} \tag{C3}$$

$$\begin{aligned} F_1 = & -\beta^{-1} \ln \big(d^3 e^{-\beta V_1^{AB} Z_1} e^{-\beta V_2^{AB} Z_2} \big) \\ & - \beta^{-1} \ln \big[e^{-\beta V_1^{AA}(Z_1/2d^3-Z_1)} e^{-\beta V_2^{AA}(Z_2/2d^3-Z_2)} \big], \end{aligned} \tag{C4}$$

TABLE III. Exact calculation of the free energy of a first-NN interaction model in the dilute limit at $T = 1.5T_c$. The free energy unit is β^{-1}.

d	$F_{2,0}$	F_2	$F_{1,1}$	F_1
3	−2.64321	−2.66593	−3.24128	−1.60784
4	−4.28958	−4.29742	−4.94995	−2.47089

where

$$W_1 = \frac{Z_1}{2}d^3 - 2d^2, \quad W_2 = \frac{Z_2}{2}d^3 - 2d^2, \tag{C5}$$

$$X_1 = 4d^2, \quad X_2 = 8d^2, \tag{C6}$$

$$Y_1 = \frac{Z_1}{2}d^3, \quad Y_2 = \frac{Z_2}{2}d^3. \tag{C7}$$

This leads to

$$\begin{aligned}\kappa_1 = \frac{-d^8\beta^{-1}}{4}\Bigg(\ln\left\{\left[\frac{d^3(d^3-1)}{2} - W_1 - W_2\right] + W_1 e^{-\beta\Omega_1}\right.\\ \left. + W_2 e^{-\beta\Omega_2}\right\} - \ln\left\{\left[\frac{d^3(d^3-1)}{2} - Y_1 - Y_2\right] + Y_1 e^{-\beta\Omega_1}\right.\\ \left. + Y_2 e^{-\beta\Omega_2}\right\} - \ln[(d^6 - X_1 - X_2) + X_1 e^{-\beta\Omega_1}\\ + X_2 e^{-\beta\Omega_2}] + \ln(d^6)\Bigg),\end{aligned} \tag{C8}$$

where we have defined the ordering energies

$$\Omega_1 = V_1^{AA} + V_1^{BB} - 2V_1^{AB}, \tag{C9}$$

$$\Omega_2 = V_2^{AA} + V_2^{BB} - 2V_2^{AB}. \tag{C10}$$

In the case of a first-NN interaction model, we obtain the values presented in Table III.

---

[1] E. Clouet, L. Laé, T. Épicier, W. Lefebvre, M. Nastar, and A. Deschamps, Nature Mater. **5**, 482 (2006).

[2] F. Soisson and C.-C. Fu, Phys. Rev. B **76**, 214102 (2007).

[3] Mao, C. K. Sudbrack, K. E. Yoon, G. Martin, and D. N. Seidman, Nature Mater. **6**, 210 (2007).

[4] T. Jourdan, F. Soisson, E. Clouet, and A. Barbu, Acta Mater. **58**, 3400 (2010).

[5] T. Jourdan, J.-L. Bocquet, and F. Soisson, Acta Mater. **58**, 3295 (2010).

[6] G. Boussinot, Y. Le Bouar, and A. Finel, Acta Mater. **58**, 4170 (2010).

[7] G. Boussinot, A. Finel, and Y. Le Bouar, Acta Mater. **57**, 921 (2009).

[8] M. Cottura, Y. Le Bouar, A. Finel, B. Appolaire, K. Ammar, and S. Forest, J. Mech. Phys. Solids **60**, 1243 (2012).

[9] A. Gaubert, A. Le Bouar, and A. Finel, Philos. Mag. B **90**, 375 (2010).

[10] K. Kaski, K. Binder, and J. D. Gunton, Phys. Rev. B **29**, 3996 (1984).

[11] J. S. Langer, M. Bar-on, and H. D. Miller, Phys. Rev. A **11**, 1417 (1975).

[12] Q. Bronchart, Y. Le Bouar, and A. Finel, Phys. Rev. Lett. **100**, 015702 (2008).

[13] F. Soisson and G. Martin, Phys. Rev. B **62**, 203 (2000).

[14] Y. Le Bouar and F. Soisson, Phys. Rev. B **65**, 094103 (2002).

[15] F. Soisson, A. Barbu, and G. Martin, Acta Mater. **44**, 3789 (1996).

[16] S. Schmauder and P. Binkele, Comput. Mater. Sci. **24**, 42 (2002). ’

[17] G. E. Murch and R. J. Thorn, in *Proceedings of the 1976 International Conference on Computer Simulation for Materials Applications, Gaithersburg, MD, USA, 19-21 April 1976* (Nat. Bur. Standards, Washington, DC, USA, 1976), pp. 245–51.

[18] H. Meirovitch and Z. Alexandrowicz, Mol. Phys. **34**, 1027 (1976).

[19] D. P. Landau and K. Binder, *Monte Carlo Simulation in Statistical Physics* (Cambridge University Press, Cambridge, UK, 2000).

[20] N. Metropolis, A. W. Rosenbluth, M. N. Rosenbluth, and A. H. Teller, J. Chem. Phys. **21**, 1087 (1953).

[21] M. Plapp, Philos. Mag. **91**, 25 (2011).

[22] H. Furukawa and K. Binder, Phys. Rev. A **26**, 556 (1982).

[23] J. Cahn and J. Hilliard, J. Chem. Phys. **28**, 258 (1958).

[24] J. D. Gunton and M. Droz, *Introduction to the Theory of Metastable and Unstable States*, Lecture Notes in Physics, Vol. 183 (Springer, New York, 1983).

[25] D. Le Floc'h, T. Saha-Dasgupta, and A. Finel, Comput. Mater. Sci. **8**, 192 (1997).